Turkish Journal of Physics

http://journals.tubitak.gov.tr/physics/

Research Article

Turk J Phys
(2017) 41: 25 – 40

doi:10.3906/fiz-1604-12

Investigating the instability of the torus around the black hole in the presence of the radial and angular velocity perturbations

Orhan DÖNMEZ*
College of Engineering and Technology, American University of the Middle East (AUM), Egaila, Kuwait

Received: 11.04.2016 • **Accepted/Published Online:** 20.09.2016 • **Final Version:** 02.03.2017

Abstract: We have performed the numerical simulation of the perturbed relativistic torus around the black hole by solving the general relativistic hydrodynamics equations on the equatorial plane. We have monitored the different simple models by applying the radial and angular velocity perturbations to the steady state torus around the black hole. The instabilities are triggered by adding the subsonic velocity fields over the radial and angular velocities of the stable torus. We have found the disk instability so-called the Papaloizou-Pringle instability and excited modes of the Quasi-Periodic Oscillations (QPOs) in the thin disk approximation case. The significant oscillations and oscillation modes in the mass accretion rates are observed around the rotating black hole with a radial velocity perturbation. The angular velocity perturbation can not create the significant variations and QPOs in the nonselfgravitating relativistic torus around the nonrotating and rotating black holes. The results observed from the radial velocity perturbation might be used to explain the Papaloizou-Pringle instability observed in NGC 1068

Key words: numerical relativity, black hole; torus, velocity perturbation, Papaloizou-Pringle instability, quasi-periodic oscillation

1. Introduction

The tori around the black holes are expected to be formed in different astrophysical scenarios such as binary merging of the compact objects, gravitational collapse of the massive stars and supernova explosions[1,2]. The numerical studies related to the torus and accretion disk around the nonrotating and rotating black holes allow to find out the oscillatory properties of these systems. In order to understand the instabilities and oscillation properties of the black hole-torus system, the numerical solutions of the relativistic equations have been proposed in the last few decades. The dynamical responds of the torus to the internal or external perturbation could be a source of instability and Quasi-Periodic Oscillations (QPOs) observed in the astrophysical phenomena. Since the oscillation epicyclic frequencies are strongly related with the black hole spin and mass, the instabilities and QPOs could be used to constrain the black hole properties[1,3,4]. On the other hand, we might also deduce the properties of the strong general relativistic region and it will give an opportunity to compare the various theories of the gravity[5-8].

The numerical simulations of perturbed accretion torus around the compact object along the radial direction had been performed by[9] and found that the appropriate epicyclic frequencies were observed in the radial and vertical directions. The applying the periodic perturbation in time excited the vertical motion in a nonlinear way. Many attempts have been made during the few decades to explain the interaction of the

*Correspondence: orhan.donmez@aum.edu.kw

black hole-torus system, instabilities, and QPOs observed from $X-$ray data[10-15]. The persistent lopsided distribution and strong noncircular motion in an astrophysical system can be strong evidence to explain the nature of the detectable gravitational waves[16]. However, we need to put more efforts to understand these astrophysical phenomena. Therefore, our goal in this paper is to introduce new mechanism by perturbing the radial and angular velocities of the initially stable torus and then we will have an opportunity to explain the physics of these phenomena.

In this work, the effect of perturbation onto the black hole-torus system is studied by using the numerical solution of the general relativistic hydrodynamical equations on a fixed background space-time. The results presented in here only include the hydrodynamics effects in the presence of the radial and angular velocity perturbations onto the stable torus around the nonrotating and rotating black holes. The effects of the magnetic field, viscosity, and radiation on the system have not been taken into account in our calculations. The paper is organized as follows: we give the formulation, numerical setup, boundary and initial conditions, and introduce the initial setup of the relativistic torus in Section 2. In Section 3, the numerical results are given and discussed. The outcomes of the respond of the black hole-torus system to radial and angular velocity perturbations and QPOs due to the oscillation of the torus are presented. Finally, Section 4 concludes the numerical results. We use geometrized unit, $G = c = 1$ and the space-time signature $(-,+,+,+)$ are used throughout the paper.

2. Equations, Numerical Setups, Initial and Boundary Conditions

2.1. Governing Equations

We consider a nonself gravitating and unmagnetized tori with a perfect fluid equation of state around the nonrotating and rotating black holes. In order to model the instabilities and QPOs produced from interaction of the black hole with a torus due to the perturbed torus, the General Relativistic Hydrodynamical (GRH) equations are solved by using the fixed space-time metric. The GRH equations are given as

$$\nabla_\mu J^\mu = 0, \quad \nabla_\mu T^{\mu\nu} = 0, \tag{1}$$

where $J^\mu = \rho u^\mu$ is a current density and $T^{\mu\nu} = \rho h u^\mu u^\nu + P g^{\mu\nu}$ is a stress-energy-momentum tensor for a perfect fluid. To use the conservative properties of hydrodynamical equations and to preserve it during the evolution, the conserved form of Eq. 1 can be written in the following form by using the $3+1$ formalism[17]

$$\frac{\partial \mathbf{U}}{\partial t} + \frac{\partial \mathbf{F}^r}{\partial r} + \frac{\partial \mathbf{F}^\phi}{\partial \phi} = \mathbf{S}\ , \tag{2}$$

where $\mathbf{U}$, $\mathbf{S}$, $\mathbf{F^r}$ and $\mathbf{F}^\phi$ are the conserved variable, source term and fluxes defined for the radial and angular directions at equatorial plane, respectively. These quantities can be represented depending on the fluid and thermodynamical variables. More detailed explanations about the GRH equations and their conserved form are given in [17,18]. The conserved variables and fluxes can be explicitly written in terms of the velocity of fluid and Lorenz factor. The source term is represented as a function of the space-time metric $g^{\mu\nu}$, lapse function α, Christoffel symbol $\Gamma^\alpha_{\mu\nu}$, the stress-energy tensor $T^{\mu\nu}$, and the determinant of three metric γ_{ij}. While the three-velocity is given as $v^i = u^i/(\alpha u^t)$ at where u^μ is called the four-velocity, the Lorenz factor is represented with $W = \alpha u^0 = (1-\gamma_{ij}v^i v^j)^{-1/2}$. The detailed representation of GRH equation on a curved fixed background space-time at equatorial plane is given in [18,19].

2.2. Initial Setups and Definition of the Physical Boundaries

In order to model the perturbed torus, we have solved the GRH equations at the equatorial plane around the black hole. We have used the code which carries out the numerical simulation by using the high resolution shock capturing scheme and it is explained in detail by [18-20]. The standard Γ law equation of state is used to compute the pressure of the matter. The perfect fluid equation of state gives the relations among pressure, the rest-mass density and internal energy of the gas, $P = (\Gamma - 1)\rho\epsilon$ with $\Gamma = 4/3$. After setting up the stable torus with a constant specific angular momentum inside the region, $r_{in} < r < r_{max}$, we have to also define the vacuum with some negligible values of all parameters. The low density atmosphere, $\rho_{atm} = 10^{-8}\rho_c$, is used in the outside of the torus but inside the computational boundaries. The other variables of atmosphere are pressure $p_{atm} = 10^{-8}p_c$, radial velocity $v^r = 0.0$ and angular velocity $v^\phi = 0.0$. The variables ρ_c and p_c represent the maximum density and pressure values at a well defined radial and angular coordinates for the stable torus, respectively. The numerical evolution of the black hole-torus system without any perturbation showed that the dynamic of steady-state torus was uninfluenced by the presence of the defined atmosphere[10]. The general form of the Kerr metric in Boyer-Lindquist coordinates is used to set up the black hole at the center of computational domain using a uniformly spaced grid along radial r and angular ϕ directions. The computational boundaries are located at $r_{min} = 2.8M$ and $r_{max} = 200M$ for the nonrotating, and $r_{min} = 1.7M$ and $r_{max} = 200M$ for the rotating black holes while ϕ goes from 0 and 2π. The number of zones used along the radial and angular directions are $(N_r \ X \ N_\phi) = (3072 \ X \ 256)$.

The initial torus is in a steady state at $t = 0$ with a radial v^r and an angular v^ϕ velocities. The radial and angular velocity profiles of the stable tori around the non-rotating and rotating black holes are given in [21-24]. The torus is perturbed by adding a velocity field along the radial and angular directions, seen in Table. The new values of the velocities after the perturbation are given in the last two columns of the Table. The magnitudes of the perturbations added to the velocity fields are subsonic and they are proportional with the original velocities of the steady state torus and the radial coordinate. The perturbation of the radial velocity is handled by adding the power law function to the original radial velocity of the stable torus. The perturbation of the radial velocity with a power law is needed to have a right profile for radial velocity within the torus around the black hole.

The physical boundaries have to be defined correctly to avoid the unwanted oscillations. So the outflow boundary condition is set up at r_{min} and r_{max} in radial direction. The zeroth-order extrapolation is used to fill the values of all variables. While the radial velocity of matter v^r should be bigger than zero at the outer boundary, it must be less than zero at the inner boundary. The boundary along the angular direction is handled by using the periodic boundary condition.

2.3. Dynamics of the Stable Torus

The analytic definition of the nonself-gravitating relativistic torus for a test fluid was first studied by [25]. It was found a sharp cusp for marginally stable accreating disc located at an equatorial plane around the black hole. Later, the torus with a perfect fluid equation of state was numerically analyzed in detail[21-24]. The polytropic equation of state $P = K\rho^\Gamma$ was used to build an initial steady state torus in hydrodynamical equilibrium with the values given in Table. The matter of the torus is rotating in a circular orbit with nongeodesic flow between inner r_{in} and outer r_{max} boundaries. The $\Gamma = 4/3$ mimics a degenerate relativistic electron gas. The centrifugal and gravitational forces are balanced by significant internal pressure to maintain the system in hydrodynamical equilibrium.

Table. Initial values of radial and angular velocities for each model. From left to right: First column represents the model name, a/M is the spin parameter of the black hole, the radial (v_n^r) and angular (v_n^ϕ) velocities of the torus which are used as a perturbation in the first time step of the simulation. The total time of the simulations varies depending on models.

Model	$\frac{a}{M}$	v_n^r	v_n^ϕ
$PT-M_1$	0.0	v^r	$v^\phi+0.1v^\phi$
$PT-M_2$	0.0	v^r	$v^\phi+0.4v^\phi$
$PT-M_3$	0.0	$v^r+\frac{1}{r^3}$	v^ϕ
$PT-M_4$	0.0	$v^r+\frac{1}{r^2}$	v^ϕ
$PT-M_5$	0.0	$v^r+\frac{2}{r^2}$	v^ϕ
$PT-M_6$	0.0	$v^r+\frac{1}{r}$	v^ϕ
$PT-M_7$	0.9	v^r	$v^\phi+0.1v^\phi$
$PT-M_8$	0.9	v^r	$v^\phi+0.2v^\phi$
$PT-M_9$	0.9	$v^r+\frac{0.05}{r^2}$	v^ϕ
$PT-M_{10}$	0.9	$v^r+\frac{0.1}{r^2}$	v^ϕ
$PT-M_{11}$	0.9	$v^r+\frac{0.5}{r^2}$	v^ϕ

The torus around the black hole may be formed as a consequence of merging of the compact binaries (merging of the black holes, neutron stars or their mixed binaries), gravitational collapse of massive star, or supernova explosions. These phenomena propose that we may have a torus in nonequilibrium after it is formed. In order to understand the physical nature of an unstable black hole-torus system and perturbation of the torus by any small displacement of the radial or angular velocity, we use the initial conditions for a nonself gravitating-unmagnetized perfect-fluid torus orbiting around a black hole using the formulations given by [22,24].

The values of the physical variables for the stable torus are: the highest density of the torus, the mass ratio of the black hole-torus, the polytropic constant, the constant specific angular momentum, inner and outer radii of the torus, cusp location, and orbital period at r_c are $\rho_c = 1.140$ x 10^{-4}, $M_t/M_{BH} = 0.1$, $K = 4.969$ x 10^{-2}, $\ell_0 = 3.80$, $r_{in} = 4.57$ and $r_{out} = 15.889$, $r_{cusp} = 4.57$, $t_{orb} = 151.6$ and $r_c = 8.35$, respectively, around the non-rotating black hole. For the rotating black hole $(a = 0.9)$, the parameters are $M_t/M_{BH} = 0.1$, $\rho_c = 1.140$ x 10^{-4}, $K = 4.969$ x 10^{-2}, $\ell_0 = 2.6$, $r_{in} = 1.78$ and $r_{out} = 19.25$, $r_{cusp} = 1.78$, $t_{orb} = 39.4$ and $r_c = 3.4$ (see Table). r_c represents the location of the maximum density of the torus along the radial coordinate.

3. Numerical Results

In this section, we investigate the respond of the torus to the radial and angular velocity perturbations around the nonrotating and rotating black holes. The evolution times of the models vary from model to model depending on the disk instabilities and relaxation times. We have studied the torus dynamics and their instabilities for various values of perturbations given in Table and compared them to have a deep understanding of the influence of the perturbations on the torus dynamic.

In order to understand the properties of the torus dynamics and instability we should compute the time-dependent analysis of the mass accretion rate. The mass accretion rate is computed in spherical coordinate at the equatorial plane by using the following expression

$$\frac{dM}{dt} = \int_0^{2\pi} \alpha\sqrt{\gamma}\rho u^r d\phi, \tag{3}$$

where α, γ, ρ, and u^r are the lapse function, the determinant of the three-matrix, density of the torus, and four-velocity along the radial coordinate, respectively.

3.1. Perturbed Torus Around the Nonrotating Black Hole

The radial and angular velocity perturbations can cause the oscillation of the torus potential well. In order to see the effect of the angular velocity perturbation, we increase the angular velocity of the stable torus from 10%-40% and compute the mass accretion rate using the Eq. 3. It is seen in Figure 1 that the mass accretion rate oscillates with very low amplitude for the models $PT-M_1$ and $PT-M_2$. The angular momentum deformation of the stable torus initially gives a first kick and then the torus maintains its dynamical structure during the evolution around the nonrotating black hole. The time evolution of the mass accretion rate computed at $r=6M$ is displayed in Figure 2 for the same models. More detailed insights have been seen at the early time of numerical simulation. The greater value of the perturbation for the angular velocity can let the gas move inward from point $r=6M$. So the stable torus is destroyed in a short time scale which is less than 2 orbital periods. The case with a small angular velocity perturbation can allow the torus to oscillate during the evolution with a certain frequency. But the amplitude of oscillation is significantly low.

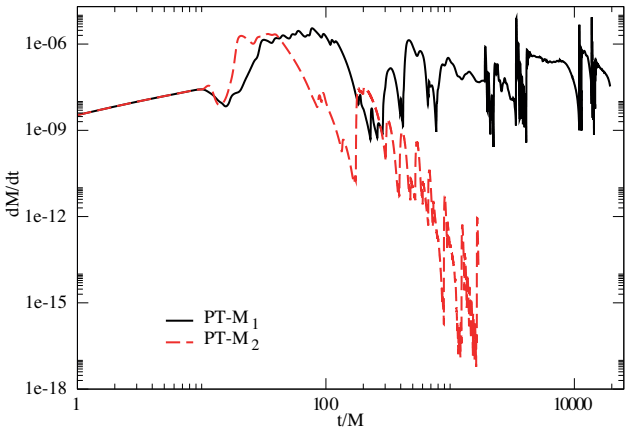

Figure 1. The mass accretion rate computed at the inner boundary of the torus, $(r_{min}=2.8M)$, around the nonrotating black hole $a=0.0$ is plotted for the perturbed torus, taking into account of the deformation due to increased angular momentum of the initial torus. While the black straight line is representing the oscillating mass accretion rate in case of angular velocity of the stable torus increased by a ten percent, the red dashed line is for forty percent increasing in the angular velocity. The mass accretion rate of the model $PT-M_1$ having an initial perturbation for angular velocity $v_n^\phi = v^\phi + 0.1v^\phi$ oscillates around a certain point but the torus is more destroyed for larger value of the perturbed angular velocity which is given in model $PT-M_2$ after the less than 13 orbital period.

The perturbations in the radial and angular velocities describe the different global oscillation properties of the torus. It is found that the radial velocity perturbation can significantly cause a bigger oscillation when we compare with the angular velocity perturbation, seen in Figure 3. The oscillation of the mass accretion rate for models $PT-M_3$, $PT-M_4$, $PT-M_5$ and $PT-M_6$ is given in Figure 3. The oscillation amplitude grows after $t=100M$ and it dumps a significant amount of matter inside the black hole at the early time of simulation. But it reaches to a quiescent state around $t=1000M$ and restores the quasi steady state cases with a lower density.

More detailed structures of the torus can be inferred from Figure 4 for model $PT-M_4$. The logarithmic

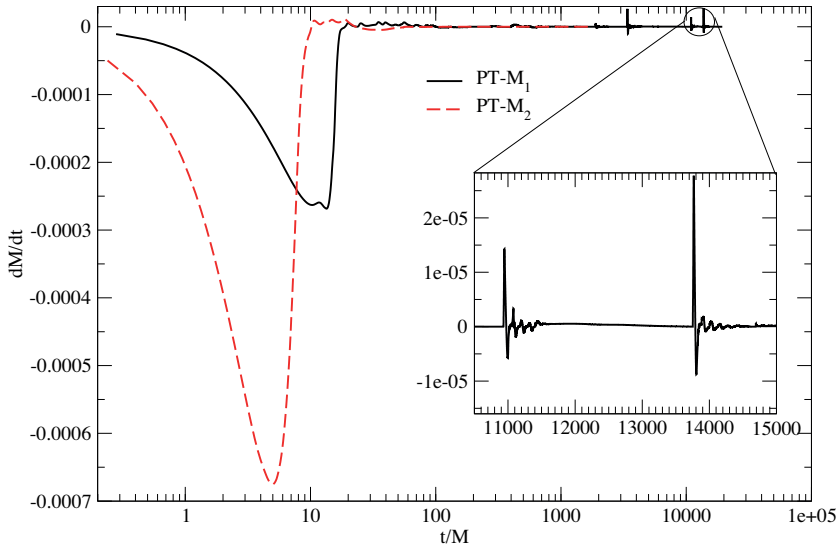

Figure 2. Same as Figure 1 but it is computed at $(r = 6M)$. The bigger value of perturbation for angular velocity can let the gas move outward from point $r = 6M$ until $t = 10M$. So the stable torus is destroyed in a short time scale which is less than 2 orbital periods. The case with a smaller angular velocity perturbation can allow the torus to oscillate during the evolution with a certain frequency.

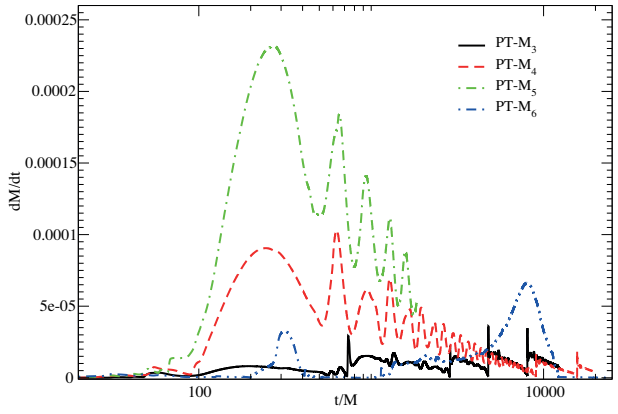

Figure 3. Same as Figure 1 but for models $PT - M_3$, $PT - M_4$, $PT - M_5$ and $PT - M_6$. The perturbation is applied by considering the deformation due to the radial velocity of the torus at the first time step of simulation.

rest mass density of the perturbed torus around the nonrotating black hole is given as a function of time. At $t = 0$, the torus is initially at a steady state. The instability is created and the mass is accreated toward to the black hole just after the perturbation is applied to the radial velocity. After $t = 15108M$, it looses some of its mass and then almost reaches a new equilibrium position. During this process, it makes a quasi-periodic oscillation.

3.2. Perturbed Torus Around the Rotating Black Hole

Investigating the disk oscillation and dynamic around the rotating black hole may provide more insights about the quasi-periodic behavior of the torus close to the black hole. To study the oscillation and quasi-periodic

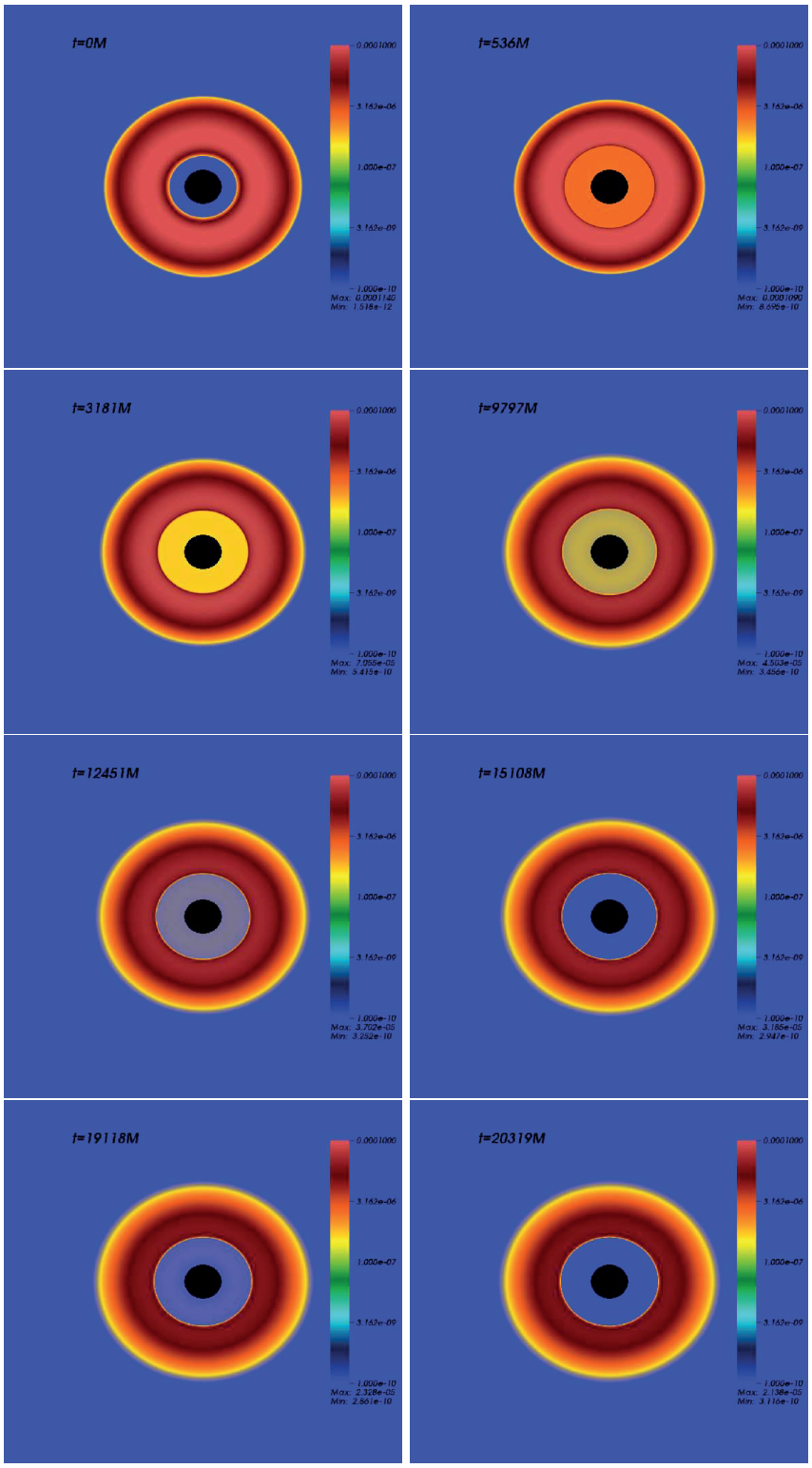

Figure 4. The logarithmic rest-mass density of the perturbed torus around the nonrotating black hole for model $PT-M_4$. Even though the physical outer boundary of computation domain is replaced at $[Xmax, Ymax] = [200M, 200M]$. The outer boundary of given color plot is $[Xmin, Ymin)] \rightarrow [Xmax, Ymax)] = [-30M, 130M] \rightarrow [30M, 30M]$.

behavior of the torus, we have performed the numerous of numerical simulations with different values of the radial and angular velocities around the Kerr black hole. Figure 5 shows the mass accretion rate around the Kerr black hole with a rotation parameter $a = 0.9$ for models $PT - M_7$ and $PT - M_8$. The oscillatory behavior of the perturbed torus is established after a few orbital periods for the angular velocity perturbation. But the oscillation amplitude is smaller for the torus which is perturbed with a higher angular velocity. It happens due to the more dumped matter at the early times of simulation.

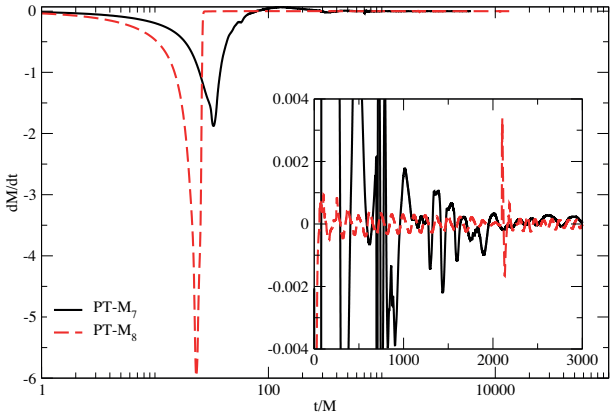

Figure 5. The mass accretion rate from the perturbed torus around the rotating black hole $a = 0.9$ for models $PT - M_7$ and $PT - M_8$ is plotted at $r = 6M$.

It is obvious from Figure 6 that the modes are excited from the radial velocity perturbation. The mass accretion rate shows the more oscillatory behavior during the evolution for models $PT - M_9$, $PT - M_{10}$ and $PT - M_{11}$. The presence of radial and orbital modes of oscillation is expected. Our numerical results show that the radial mode is more excited than the orbital mode. The dynamical change of the torus structure as a function of time is given in Figure 7. Even though we observe some quasi-periodic behaviors of the torus and the mass is accreated toward to the black hole, the dynamic of the torus and its rest mass density almost remain constant during the evolution.

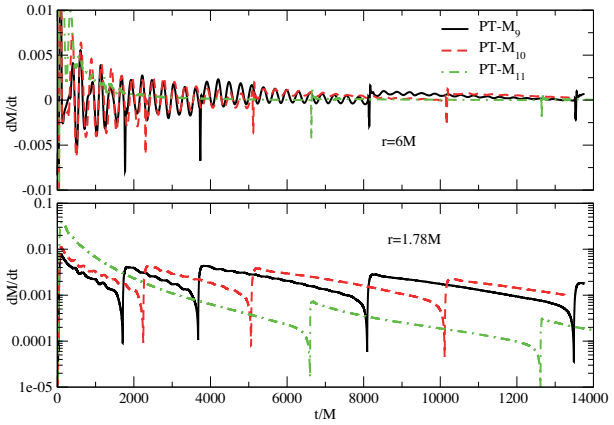

Figure 6. Same as Figure 5 but for models $PT - M_9$, $PT - M_{10}$ and $PT - M_{11}$. The accretion rates are computed at the inner radius of the torus $(r = 1.78M)$ and at $r = 6M$.

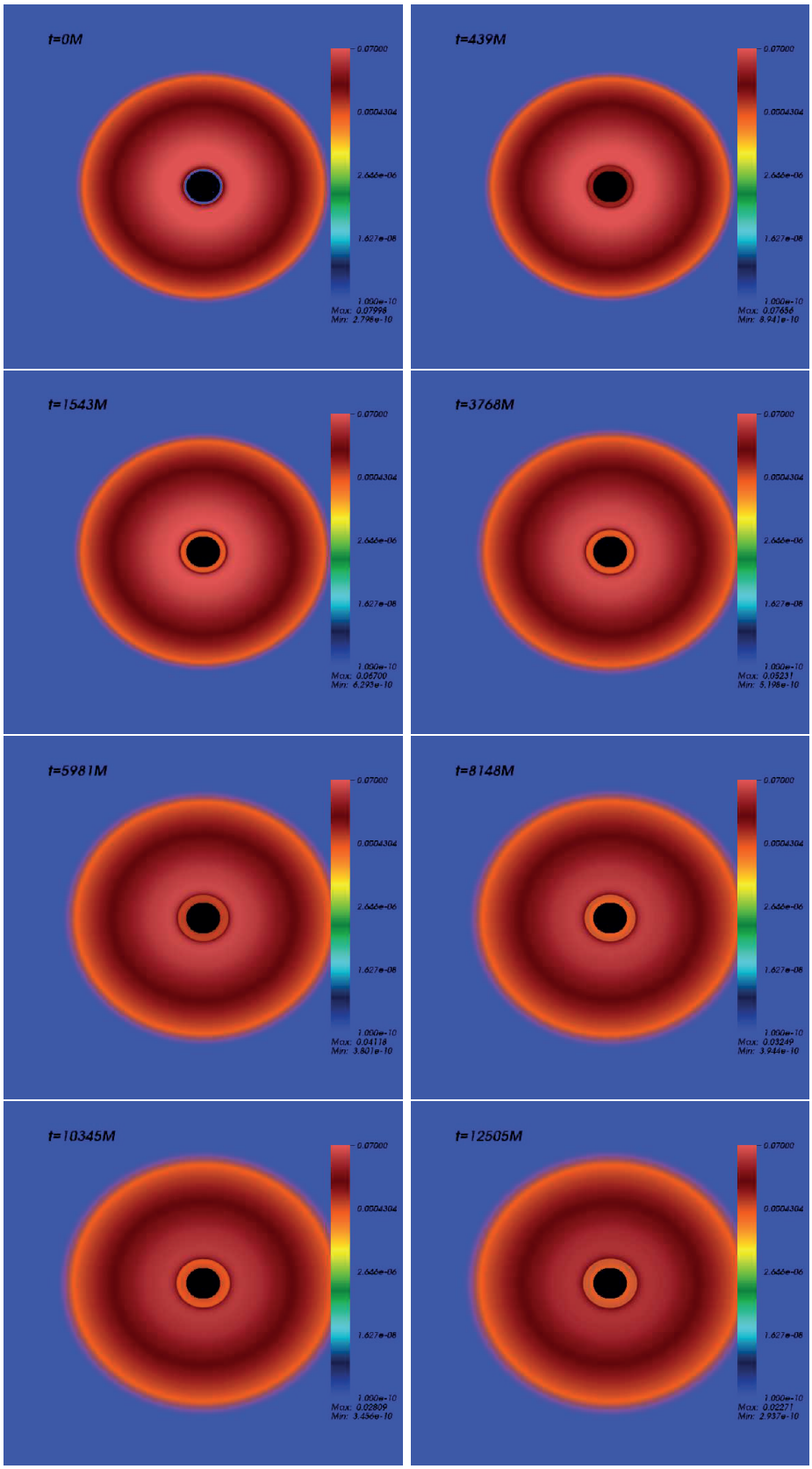

Figure 7. Same as Figure 4 but it is for model $PT-M_{10}$ around the rotating black hole with $a=0.9$.

3.3. Fourier Mode Analysis of the Instability of the Torus

Numerically, the nonaxisymmetric instabilities can be detected and characterized by using the perturbation of the torus around the black hole. Computing the saturation point and the azimuthal wave number m will allow us to determine the type of instability. It can be handled by performing the numerical computation of the Fourier power in density. The Fourier modes $m = 1$ and $m = 2$ and their growth rates can be obtained at the equatorial plane by calculating imaginary and real parts of the mode power and it is given as[26],

$$Im(w_m(r)) = \int_0^{2\pi} \rho(r,\phi) sin(m\phi) d\phi, \tag{4}$$

$$Re(w_m(r)) = \int_0^{2\pi} \rho(r,\phi) cos(m\phi) d\phi, \tag{5}$$

So the mode power is defined from the Eqs.4 and 5 as

$$P_m = \frac{1}{r_{out} - r_{in}} \int_{r_{in}}^{r_{out}} ln\left([Re(w_m(r))]^2 + [Im(w_m(r))]^2\right) dr, \tag{6}$$

where r_{in} is the inner radius and r_{out} is the outer radius of the initially formed stable torus.

The nonaxisymmetric instability can grow on a dynamical time scale and so-called Papaloizou-Pringle instability [27,28]. The perturbation of the black hole-torus system can cause to arise a Papaloizou-Pringle instability observed previously by [10-12]. In this section, we numerically prove the occurrence of Papaloizou-Pringle instability in the presence of the radial and angular velocity perturbations around the nonrotating black hole. As it is seen in Figure 8, we do not observe any Papaloizou-Pringle instability for models $PT - M_1$ and $PT - M_2$ but the instability is weakly observed for the models $PT - M_3$, $PT - M_4$, $PT - M_5$ and $PT - M_6$, seen in Figure 9. The saturation points are created around $t = 100M$ and then the Papaloizou-Pringle instability starts to disappear around $t = 10000M$ for the models $PT - M_4$ and $PT - M_6$. In order to maintain the instability, the waves must be kept inside the torus by reflecting it at inner and outer boundaries.

In order to understand the strengthness of the global oscillation modes, we plot the $m = 1$, $m = 2$ and $m = 3$ growth modes of model $PT - M_3$, seen in Figure 10. It is noted that all modes have almost same strength. The Papaloizou-Pringle instability is seen in the early time of simulation but it disappears later.

It is obvious from the growth rate of the Papaloizou-Pringle instability around the nonrotating black hole that the nonaxisymmetric instability do not grow in the tori orbiting around the black hole. But it is seen in Figure 11 that the nonaxisymmetric instability mode grows especially for models $PT - M_7$, $PT - M_8$, $PT - M_9$, and $PT - M_{10}$ around the rotating black hole. The Papaloizou-Pringle instability structure persists for enough time which is longer than the dynamical time of the torus. This type of instability would become a stronger emitter with a large amplitude[16]. After the radial and angular perturbations are applied onto the black hole-torus system, the instability grows in the first orbital period and then it reaches a peak value called saturation point. Finally, it settles to an approximately nonzero constant value for all models given in Figure 11.

3.4. QPOs from the oscillating Torus

It is interesting to define the spectra of the oscillating accretion disk and the torus around the black hole. The global modes and their overtones may allow us to understand the nature of oscillations observed in a perturbed

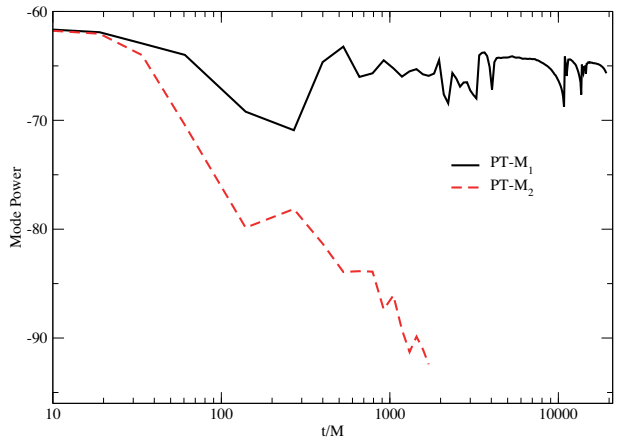

Figure 8. Evolution of $m = 1$ mode growth for models $PT - M_1$ and $PT - M_2$ around the nonrotating black hole, $a = 0.0$.

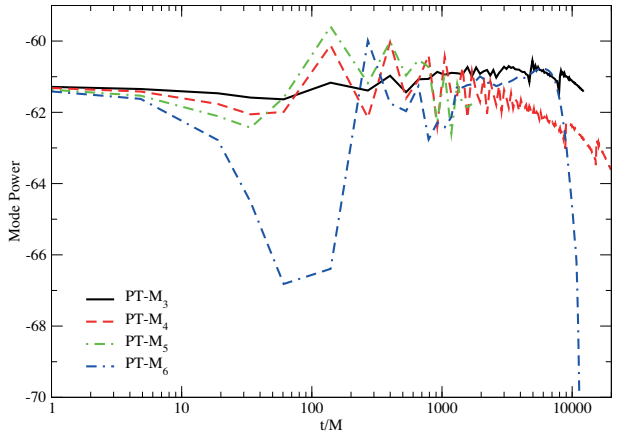

Figure 9. Same as Figure 8 but it is for $PT - M_3$, $PT - M_4$, $PT - M_5$ and $PT - M_6$.

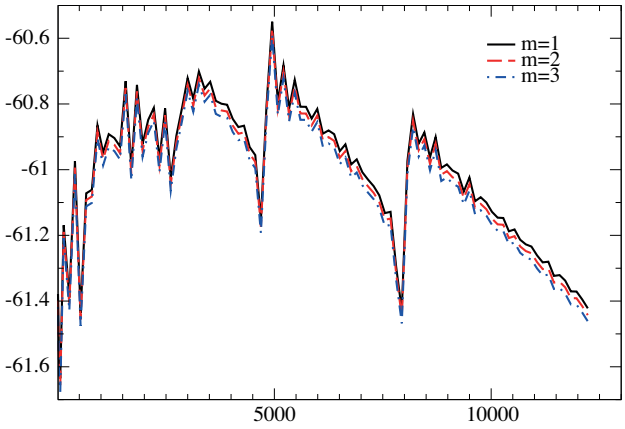

Figure 10. The growth of $m = 1$, $m = 2$ and $m = 3$ modes of model $PT - M_3$.

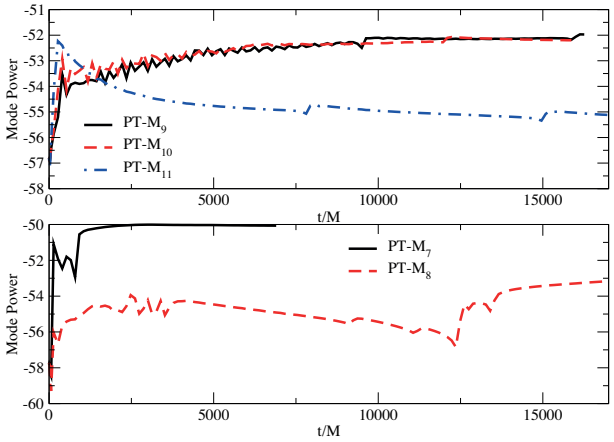

Figure 11. Same as Figure 8 but it is for the torus around the rotating black hole, $a = 0.9$ given for models $PT - M_9$, $PT - M_{10}$ and $PT - M_{11}$ in upper and for models $PT - M_7$ and $PT - M_8$ for lower panels.

system[29-31]. The physical variables and black hole parameters used in the performed numerical simulations are given in Table. The numerical results indicate that the global oscillations are observed at various frequencies. The proper time is used to compute the frequencies of the oscillating torus and the following equation is used to compute the oscillation frequency which translates the geometrized unit into Hertz relative to the black hole mass

$$f(Hz) = 2.03027 \times 10^4 \times \left(\frac{10M_\odot}{M}\right) \times f(M), \tag{7}$$

where $M_\odot$, M, $f(Hz)$, and $f(M)$ are the solar mass, mass of the black hole, frequency in Hz, and the frequency in the geometrized unit, respectively.

The parameters of the black holes, such as mass and spin, can be extracted from the power spectrum by analyzing the theory of the quasi-periodic oscillation of the black hole-torus system. There are number of proposed models to explain the observed frequencies and their relations with orbital motion and perturbation applied on the black hole-torus system. Such models may explain the nature of frequencies and their variation with the black hole mass and spin[32].

Here we have proposed QPOs from the radial and angular perturbations of the torus. Figure 12 shows the power spectrum as a function of frequency around the nonrotating black hole. The highest peaks and subsequent overtones are observed and they create 1:2:3:.. ratios for all models but the amplitudes of peaks are really low close to the order of noise level (i.e. level of background oscillation or an oscillation amplitude of the unperturbed torus around the black hole). On the other hand, the observed peaks around the rotating black hole-torus system are more powerful and the 3:2 ratio occurs in the oscillating torus due to overtone and nonlinear coupling of the overtones. The nonlinear coupling may be an important excitation mechanism of the X-ray flares[10,20,23-25,33].

By comparing the power spectrum obtained from the oscillating torus around the nonrotating and rotating black holes by using the spectral methods, it is noted that QPOs around the rotating black hole are more powerful. As seen in Figure 13, they are in the observable ranges. It is also noted that the black hole rotation parameter has a large impact on QPOs.

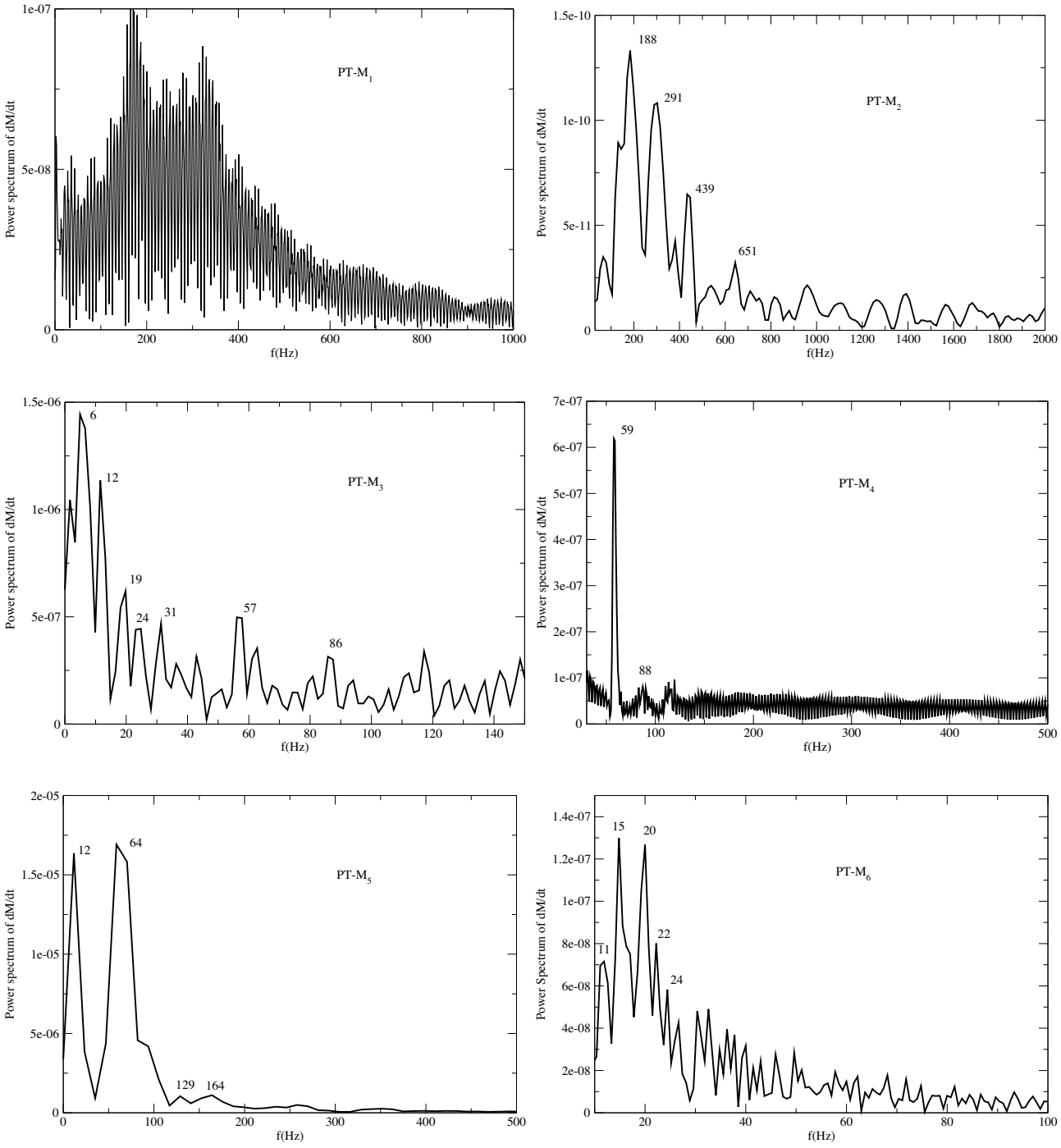

Figure 12. The power spectrum of the mass accretion rate computed at $r = 6M$ for different models around the nonrotating black hole. The arbitrary unit have been used for the power spectrum.

4. Conclusion

We have studied the effect of the radial and angular velocity perturbations on the stable torus around the nonrotating and rotating black holes. From this extent, we have numerically solved the general relativistic

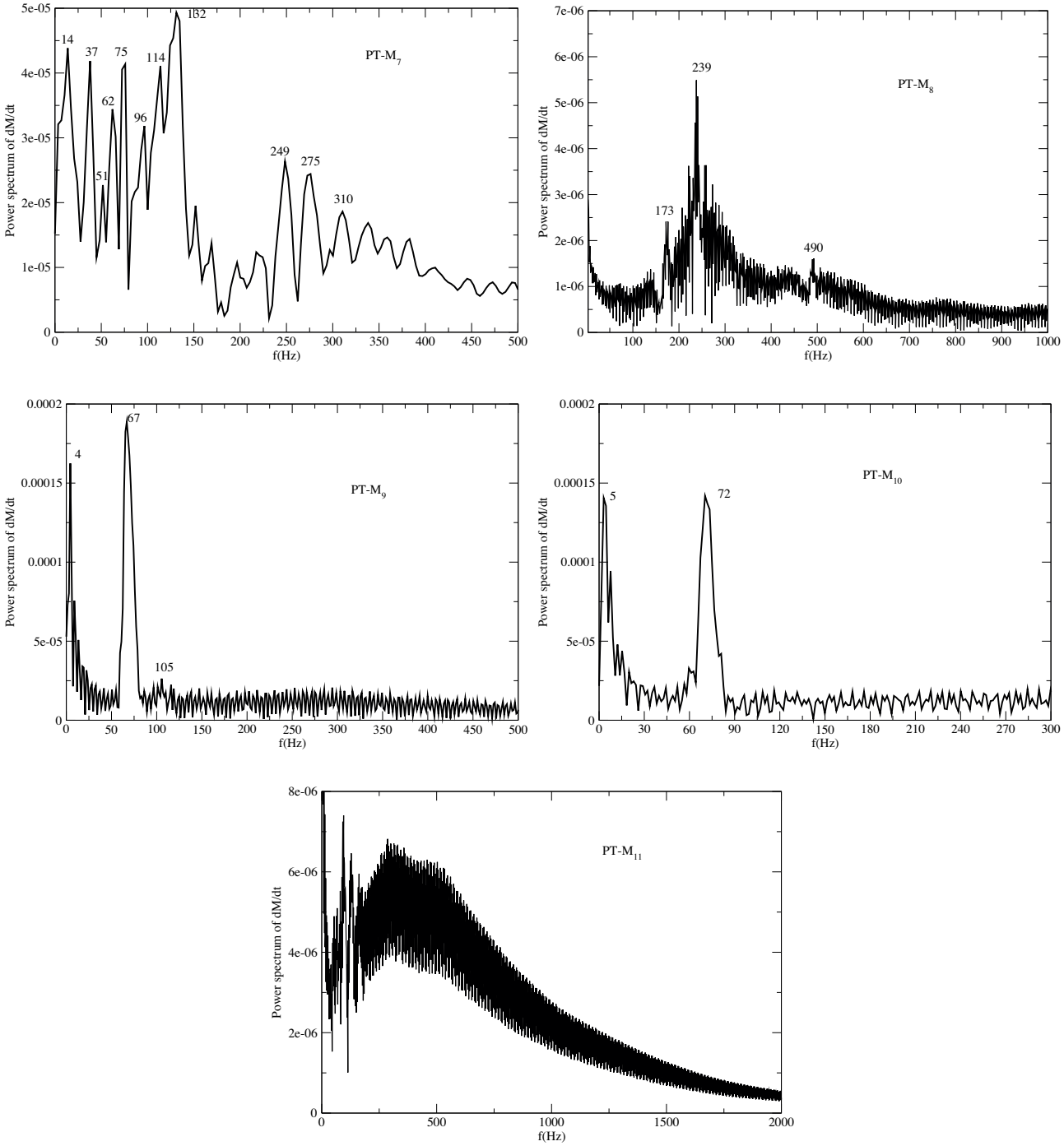

Figure 13. Same as Figure 12 but it is for the perturbed torus around the rotating black hole $a = 0.9$.

hydrodynamics equations on the equatorial plane. We have searched the instabilities and QPOs that are the consequence of the applied perturbations onto the torus and also have identified the modes and QPOs of the oscillations.

It is seen that the Papaloizou-Pringle instability arises from the interactions of the nonaxisymmetric

waves due to the perturbations of the black hole-torus system on a dynamical time-scale. We numerically prove the occurrence of Papaloizou-Pringle instability in the presence of the radial and angular velocity perturbations around the nonrotating and rotating black holes. The Papaloizou-Pringle instability in the torus around the rotating black hole is stronger and persists its structure enough time, which is longer than the dynamical time of the torus, than the instability in the torus around the nonrotating black hole. After the radial and angular perturbations are applied on the torus, the instability almost grows in the first orbital period and then it reaches to a saturation point. Finally, it settles to a nonzero constant value for all models. The latest observation indicates the evidence of Papaloizou-Pringle instability in Seyfert galaxy NGC 1068 seen by $ALMA$ [34]. The radial and angular velocity perturbations of the torus could be used to explain the nature of the instability observed in this galaxy.

The perturbed torus manifests the respond of the perturbation to all thermodynamical and hydrodynamical parameters. The power spectrum analysis of the density gives more insight about the quasi-periodic properties of the torus. In this paper, we have proposed QPOs from the radial and angular perturbations of the torus. It is shown that the 1:2:3:.. ratios are observed but the strengths of the observed peaks are really close to the order of noise level (i.e. level of background oscillation or an oscillation amplitude of the unperturbed torus around the black hole) in the case of the nonrotating black hole. However, the observed peaks around the rotating black hole-torus system are more powerful and the 3:2 ratio occurs in the oscillating torus due to overtone and nonlinear coupling of the overtones.

Our numerical approximation is addressing one of the simplest models of disk instabilities and QPOs observed in the torus around the nonrotating and rotating black holes in the hydrodynamical region. In order to come up with more certain results and compare them with the observations, we should have more realistic scenarios including the role of magnetic field and radiation.

Acknowledgments

All simulations were performed at the National Center for High Performance Computing of Turkey (UYBHM) under grant number 10022007.

References

[1] Abramowicz, M.A.; Fragile, P.C. *Living Rev. Relativity* **2013**, *16*.

[2] Abramowicz, M.A.; Calvani, M.; Nobili, L. *Nature* **1983**, *302*, 597-599.

[3] Abramowicz, M.A.; Kluzniak, W. *A&A* **2001**, *374*, L19-L20.

[4] Silbergleit, A.S.;, Wagoner, R.V.; Ortega-Rodriguez, M. *Astrophysical Journal* **2001**, *548*, 335.

[5] Johannsen, T.; Psaltis, D. *ApJ* **2011**, *726*, 11.

[6] Bursa, M.; Abramowicz, M.A.; Karas, V.; Kluzniak, W. *ApJ* **2004**, *617*, L45-L48.

[7] Bursa, M. *Astron.Nachr.* **2005**, *326*, 849-855.

[8] Montero, P.J.; Font, J.A.; Shibata, M. *PRL* **2010**, *104*, 191101.

[9] Lee, W.H.; Abramowicz, M.A.; Kluzniak, W. *ApJ* **2004**, *603*, L93.

[10] Dönmez, O. *MNRAS* **2014**, *438*, 846.

[11] Dönmez, O. *IJMPD* **2014**, *23*, 1450050.

[12] Dönmez, O. *MPLA* **2015**, *30*, 1550071.

[13] Mazur, G.P.; Zanotti, O.; Sadowski, A.; Mishra, B.; Kluzniak, W. *MNRAS* **2016**, *456*, 3245-3252.

[14] Parthasarathy, V.; Manousakis, A.; Kluzniak, W. *MNRAS* **2016**, *458*, 666-672.

[15] Torok, G.; Goluchova, K.; Horak, J.; Sramkova, E.; Urbanec, M.; Pechacek, T.; Bakala, P. *MNRAS: Letters* **2016**, *457*, L19-L23.

[16] Kiuchi, K.; Shibata, M.; Montero, P.J.; Font, J.A. *Phys. Rev. Ltt.* **2011**, *106*, 251102.

[17] Font, J. A.; Miller, M.; Suen, W.-M.; Tobias, M. *Phys. Rev. D* **2000**, *61*, 044011.

[18] Dönmez, O. *Astrophys. Spac. Sci.* **2004**, *293*, 323.

[19] Yildiran, D.; Dönmez, O. *IJMPD* **2010**, *19*, 2111-2133.

[20] Dönmez, O.; Zanotti, O.; Rezzolla, L. *MNRAS* **2011**, *412*, 1659.

[21] Nagar, A.; Font, J.A.; Zanotti, O.; de Pietri, R. *PRD* **2005**, *72*, 024007.

[22] Zanotti, O.; Rezzolla, L.; Font, J.A. *MNRAS* **2003**, *341*, 832.

[23] Zanotti, O.; Font, J.A.; Rezzolla, L.; Montero, P.J. *MNRAS* **2005**, *356*, 1371.

[24] Zanotti O.; Rezzolla, L. *MSAIS* **2003**, *1*, 192.

[25] Abramowicz, M.A.; Jaroszynski, M.; Sikora, M. *A&A* **1978**, *63*, 221-224.

[26] De Villiers, J.-P.; Hawley, J. *ApJ* **2002**, *577*, 866.

[27] Papaloizou J. C. M.; Pringle, J.E. *MNRAS* **1984**, *208*, 721.

[28] Papaloizou J.C.M.; Pringle, J. E. *MNRAS* **1985**, *213*, 799.

[29] Dönmez, O. *MPLA* **2007**, *22*, 141-157.

[30] Montero, P.J.; Zanotti, O.; Font, J.A.; Rezzolla, L. *MNRAS* **2007**, *378*, 1101.

[31] Rezzolla, L.; Yoshida, S.; Zanotti, O. *MNRAS* **2003a**, *344*, 978.

[32] Wagoner, R.V.; Silbergleit, A.S.; Ortega-Rodrguez, M. *Astrophys. J. Lett.* **2001**, *559*, L25L28.

[33] Dönmez, O. *MNRAS* **2012**, *426*, 1533-1545.

[34] Garcia-Burillo, S.; Combes, F.; Almedia, C.R.; Usero, A.; Krips, M.; Alonso-Herrero, A.; Aalto, S.; Casasola, V.; Hunt, L.K.; Martin, S. et.al. *Astrophys. J. Lett.* **2016**, *823*, L12.